Applied Catalysis B: Environmental 232 (2018) 365–370

Contents lists available at ScienceDirect

Applied Catalysis B: Environmental

journal homepage: www.elsevier.com/locate/apcatb

Insight into the synergistic effect between nickel and tungsten carbide for catalyzing urea electrooxidation in alkaline electrolyte

Lu Wang[a,*], Shangqian Zhu[b], Nebojsa Marinkovic[c], Shyam Kattel[d], Minhua Shao[b], Bolun Yang[a,*], Jingguang G. Chen[c,d,*]

[a] Department of Chemical Engineering, State Key Laboratory of Multiphase Flow in Power Engineering, Xi'an Jiaotong University, Xi'an 710049, PR China
[b] Department of Chemical and Biological Engineering, The Hong Kong University of Science and Technology, Clear Water Bay, Kowloon, Hong Kong, PR China
[c] Department of Chemical Engineering, Columbia University, New York 10027, USA
[d] Chemistry Division, Brookhaven National Laboratory, Upton, NY 11973, USA

ARTICLE INFO

Keywords:
Urea electrooxidation
Tungsten carbides
In situ FTIR
C–N bond

ABSTRACT

Tungsten carbide modified nickel (Ni-WC/C) catalyst is synthesized through the sequential impregnation method and evaluated for the electrooxidation of urea in alkaline electrolyte. Both the activity and stability of Ni are enhanced by the introduction of WC. In situ Fourier transform infrared (FTIR) measurements combined with electrochemical analysis were used to provide a better understanding of the mechanism for urea electrooxidation on the Ni-based catalysts. The formation of CO_2 and NCO^- species is detected during urea oxidation, and the synergistic effect resulting from the interaction of Ni and WC is also proposed. The Ni-WC/C electrode contributes to the improved C–N bond cleavage in urea than that on Ni/C, resulting in a higher activity. Furthermore, the introduction of WC also enhances the anti-poisoning ability, thus promoting more complete oxidation of urea to produce CO_2, which leads to a higher energy conversion efficiency than that on Ni/C. This work provides a new strategy for designing highly efficient catalysts for urea electrooxidation.

1. Introduction

To overcome energy shortage and environmental pollution, low-temperature fuel cells have attracted increasing attention as possible alternative energy devices [1,2]. Among various options for fuels, urea is a promising hydrogen carrier [3,4]. Direct urea fuel cells utilize the urea-rich wastewater or urine (containing 0.33 M urea) as fuels, which can generate electricity while simultaneously processing wastewater to produce clean water [5,6]. It may have great potential for the application in aerospace missions. For example, the urine of astronaut can be utilized as fuel rather than wastewater to supplement energy and clean water supply. More importantly, non-precious metal catalyst, such as nickel, is active for urea electrooxidation, which offers the possibility of reducing the cost of fuel cells without using precious metals [7–9]. During the electrooxidation of urea, nickel would be oxidized to NiOOH to catalyze the reaction [10,11]. However, the initial reaction kinetics is relatively slow due to the limited amount of NiOOH and the reaction rate quickly decreases. Therefore, more efficient catalysts need to be explored to achieve enhanced catalytic activity and stability toward urea electrooxidation.

Different nanostructured nickel hydroxide catalysts were synthesized, including nanosheet [12], nanowire [13] and nanotube [14], to increase the generation of active sites. To further promote the activity and stability, bimetallic or ternary Ni-based catalysts such as Ni—Rh, Ni—Pt, Ni—Ir—Pt, Ni—Co, Ni—Mn, and Ni—Zn—Co were developed by various methods [15–21]. Among these composite catalysts, electrodeposited Rh/Ni catalyst has much higher stability, and the introduction of Co could reduce the overpotential of urea electrooxidation. However, it is difficult to enhance both the activity and stability simultaneously. Also, the understandings of promotion mechanisms on the molecular level are still unclear.

Among other electrooxidation reactions, transition metal carbides (TMCs) were recently used as co-electrocatalyst to enhance the electrocatalytic activity and stability toward hydrogen, methanol and ethanol oxidation. They exhibit metallic electrical conductivity, corrosion resistance and high melting points, and interaction with active metals [22–24]. Our previous work has shown that the introduction of tungsten carbide (WC) with nickel could significantly improve the activity and simultaneously enhance the stability for urea electrooxidation [25]. Although Ni-based catalysts have been promoted for

* Corresponding authors at: Department of Chemical Engineering, State Key Laboratory of Multiphase Flow in Power Engineering, Xi'an Jiaotong University, Xi'an 710049, PR China/ Department of Chemical Engineering, Columbia University, New York 10027, USA/Chemistry Division, Brookhaven National Laboratory, Upton, NY 11973, USA.
E-mail addresses: wangluxjtu@xjtu.edu.cn (L. Wang), blunyang@mail.xjtu.edu.cn (B. Yang), jgchen@columbia.edu (J.G. Chen).

https://doi.org/10.1016/j.apcatb.2018.03.064
Received 22 September 2017; Received in revised form 17 March 2018; Accepted 19 March 2018
Available online 20 March 2018
0926-3373/

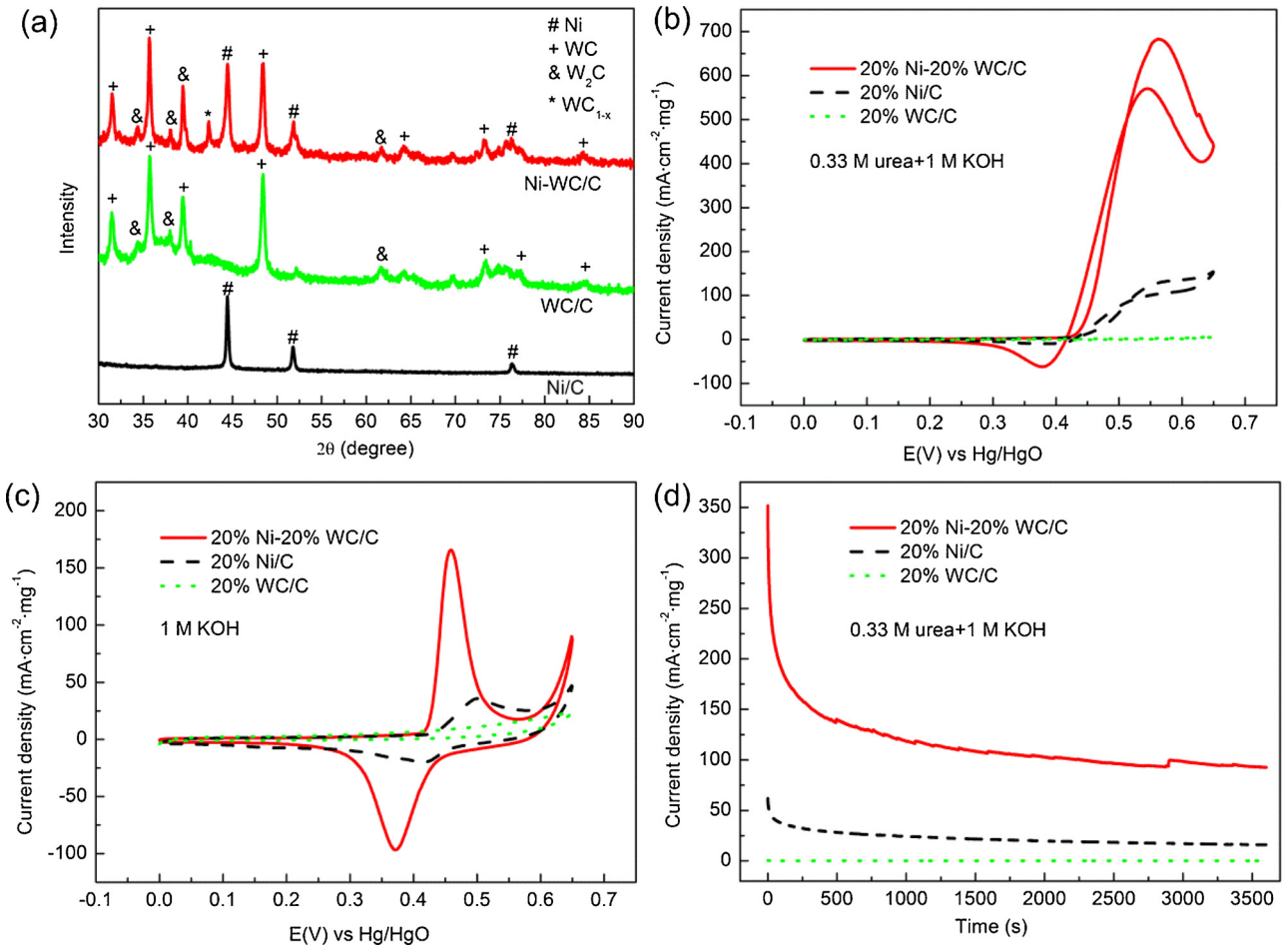

Fig. 1. (a) XRD patterns of as-prepared 20% Ni-20% WC/C and 20% Ni/C catalysts; CVs of Ni-WC/C and Ni/C electrodes in 1 M KOH in the presence (b) and absence (c) of 0.33 M urea. The scan rates were 10 mV s^{-1}; (d) Chronoamperograms of Ni-WC/C and Ni/C electrodes in 1 M KOH solution in the presence of 0.33 M urea. Applied potential was 0.5 V vs. Hg/HgO.

catalyzing urea electrooxidation through the introduction of WC, the synergistic effect between Ni and WC is not understood. With respect to the urea electrooxidation mechanism, Botte et al. proposed nickel oxyhydroxide (NiOOH) as the active form that initiates urea oxidation through a sequence of electrochemical steps, which is confirmed by in situ surface-enhanced Raman spectroscopy [26] and in situ X-ray diffraction [27]. They also predicted the possible reaction paths, products and rate-limiting step of urea decomposition with NiOOH as the catalyst by density functional theory (DFT) calculation [28]. Their DFT calculations suggested that other than the complete oxidation of urea to produce CO_2, cyanate ion (NCO^-) might also be produced in one possible pathway, which could be the reason for the low reaction rate [28]. Since NCO^- is a product of the incomplete oxidation of urea in which only one C–N bond is cleaved, the formation of NCO^- would cause lower energy conversion efficiency. Therefore, it is necessary to verify the reaction pathway for urea oxidation on the catalysts. However, there is no direct spectroscopic evidence regarding the key reaction species and intermediates during the urea electrooxidation on Ni-based catalysts. The fundamental understanding of the electrocatalytic process and enhancement mechanism of Ni by WC during the reaction in alkaline media needs to be identified in order to further improve the catalytic performance.

In situ Fourier transform infrared spectroscopy (FTIR) is a powerful tool for monitoring the key reaction species during the reaction [29,30]. In this work, in situ FTIR was combined with electrochemical measurements to bring new insight into the mechanism of urea oxidation. The formation of CO_2 and NCO^- species was detected during urea oxidation by the direct spectroscopic evidence for the first time. The synergistic effect resulting from the interaction of Ni and WC is also proposed. These findings should be of importance for designing high performance Ni-based catalysts for urea electrooxidation. Since Ni-based electrocatalysts have also been used in other types of alkaline fuel cells, such as direct alcohol and glucose fuel cells, the design strategy from the current study can also be extended to develop catalysts for these electrochemical devices.

2. Experimental methods

The Ni-WC/C catalyst was prepared using a sequential impregnation method. First, activated carbon was put in an ammonium paratungstate aqueous solution followed by a temperature-programming reduction (TPR) treatment with CH_4 and H_2 to obtain WC/C. It was then impregnated in a nickel nitrate aqueous solution with another TPR treatment to produce the Ni-WC/C catalyst. The TPR procedures were the same as reported previously [25]. XRD patterns were obtained using a Rigaku D/max-2400 with a Cu Kα radiation source to determine the crystalline structures.

All electrochemical measurements were performed in a 1 M KOH solution in the absence and presence of 0.33 M urea. The details of electrode preparation and electrochemical setup were as reported previously [25]. In brief, the cyclic voltammetry (CV) measurements were performed between 0 V–0.65 V in a conventional three-electrode cell. Nickel electrode, Hg/HgO electrode, and platinum foil were chosen as the working, reference, and counter electrodes, respectively.

Chronoamperometry (CA) measurements were carried out in a solution of 1 M KOH with 0.33 M urea at 0.5 V.

FTIR measurements were conducted with a Nicolet Nexus iS50 spectrometer equipped with a liquid nitrogen-cooled MCT detector, in a manner similar to that described previously [30]. ATR scans were recorded on a built-in diamond ATR accessory to the iS50 instrument, equipped with a dedicated DTGS detector. The in situ FTIR cell was set up using a ZnSe hemisphere window, and the same three electrodes as those for the CV measurements. The electrolyte contained 1 M of KOH in the presence of 0.33 M urea. The possible signal interference from gaseous CO_2 and water moisture was eliminated by purging the FTIR chamber by N_2. Sample single beam spectra were collected at the potential 50 mV more positive than the reference spectrum. The spectra are presented as absorbance and contain both positive and negative bands, so that positive-going FTIR bands correspond to the gain of a particular species at the sample potential relative to that at the reference, and the negative bands represent their loss. Real-time IR spectra during CO stripping measurements were also recorded. The working electrode was initially kept at 0.1 V vs RHE for 10 min in the CO-saturated 1 M KOH solution. Then Ar was purged into the cell for 20 min with potential kept at 0.1 V in order to remove the surplus of CO in the solution. The potential was then positively swept to 1.2 V vs RHE at a scan rate of 5 mV s^{-1} and the FTIR spectra were collected every 20 s.

3. Results and discussion

Fig. 1a shows the XRD patterns of Ni/C, WC/C and Ni-WC/C. Three characteristic peaks are observed in each spectrum for nickel (2θ = 44.5, 51.8, and 76.4), corresponding to Miller indices (111), (200), and (222) [31], respectively. In the presence of WC, additional XRD peaks are observed at 2θ of 31.54, 35.66 and 48.44 with the d values of 0.2834, 0.2516 and 0.1878 nm, corresponding to the (001), (100) and (101) facets of WC, respectively [32]. Other peaks are from the crystal planes of W_2C or WC_{1-x}. No peaks corresponding to W or WO_x are detected, verifying that all tungsten is in the carbide phase in the prepared catalysts.

The cyclic voltammograms (CVs) of Ni/C, WC/C and Ni-WC/C electrodes in 1 M KOH solution in the presence of 0.33 M urea are shown in Fig. 1b. No obvious oxidation current of WC/C is observed. The oxidation current of Ni-based electrodes commences at ca. 0.4 V, indicative of the electrooxidation of urea in alkaline media [33]. The Ni-WC/C catalyst gave a much higher peak current density (682.9 mA cm^{-2} mg^{-1}) for the urea electrooxidation compared to the Ni/C catalyst (154.2 mA cm^{-2} mg^{-1}) due to the synergistic effect between Ni nanoparticles and the tungsten carbides. In the absence of urea, a pair of redox peaks is observed on the Ni/C and Ni-WC/C electrodes at 0.45 and 0.37 V vs. Hg/HgO, which are due to the reversible transformation between Ni^{2+} and Ni^{3+} (Fig. 1c). On the contrary, the current peak on the electrode of WC/C is nearly negligible, confirming that the higher current observed on Ni-WC/C is not related to WC oxidation in alkaline solution. Combining the results in Fig. 1b and c, we conclude that the increasing current densities above 0.4 V in the presence of urea fall in the region where the NiOOH is generated in the 1 M KOH solution [4,34], suggesting that NiOOH is the active form for urea electrooxidation.

The electrochemical surface areas (ESAs) of the Ni-WC/C and Ni/C catalysts were estimated using the charge required to reduce NiOOH to $Ni(OH)_2$ during the cathodic sweeps from Fig. 1c [34]. The calculated results (Table 1) reveal that Ni-WC/C has a larger ESA (56.4 m^2 g^{-1}) than that of Ni/C (17.8 m^2 g^{-1}), leading to more active sites to absorb and activate urea molecules. Furthermore, the specific activity representing the intrinsic activity can be obtained by the mass activities per ESA. The Ni-WC/C catalyst also exhibits a higher specific activity (4.3 A m^{-2} Ni) than that of Ni/C (3.1 A m^{-2} Ni). These results reveal that the synergistic effect between Ni and WC contributes to the increase in the number of active sites as well as the intrinsic activity for urea electrooxidation. The stability of Ni/C and Ni-WC/C for urea electrooxidation was also investigated with chronoamperometry (CA) experiments at 0.5 V in the 0.33 M urea + 1 M KOH solution, as shown in Fig. 1d. After one hour the steady-state current density on the Ni-WC/C electrode is much higher than on Ni/C.

Table 1
ESAs, mass activities and specific activities for Ni/C and Ni-WC/C of urea electrooxidation.

Catalysts	ESAs (m^2 g^{-1})	mass activities (mA mg^{-1} Ni)	specific activities (A m^{-2} Ni)
Ni/C	17.8	54.5	3.1
Ni-WC/C	56.4	241.3	4.3

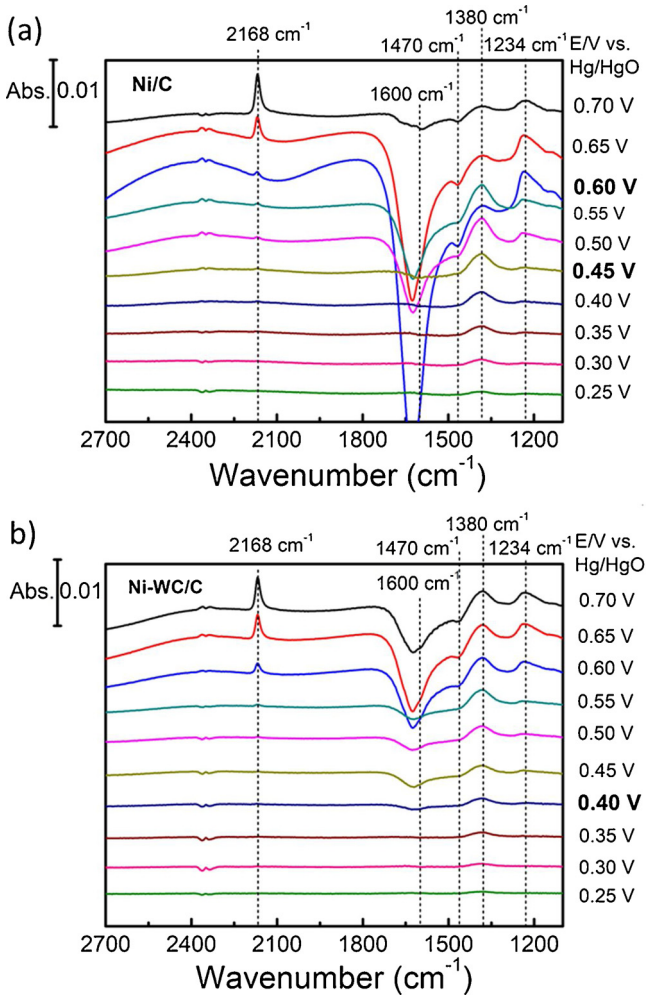

Fig. 2. Real-time FTIR spectra of (a) Ni/C and (b) Ni-WC/C electrode in the solution of 0.33 M urea + 1 M KOH during positively sweeping the potential from 0 to 0.7 V vs. Hg/HgO at a scan rate of 1 mV s^{-1}. The spectrum taken at the potential of 50 mV lower was used as the IR reference for the subsequent one.

In order to understand the origin of the enhancement in both the activity and stability by the introduction of WC, in situ FTIR study was conducted to investigate the synergistic effect from the interaction of Ni and WC. The absorbance spectra shown in Fig. 2 contain several positive and negative-going peaks, indicating accumulation and dissipation of the species at sample potential relative to that at reference, respectively. The spectra are practically featureless below 0.4 V. Above this potential, several peaks are detected. The most prominent is the

Table 2
Peak assignments for the IR spectra of urea electrooxidation.

Wavenumber (cm^{-1})	assignment
2168	NCO^- in the solution
1630	$\delta(NH_2)$ [42–44]
1600	$\delta(NH)$ [42–44]
1470	$\nu(CN)$ [42–44]
1380	$\nu(CO)$ [45]
1234	$\delta(COH) + \nu(CO_2)$ [46]
1160	$\rho(NH)$ [44]

negative-going band around 1640 cm^{-1}, which is assigned to the OH bending mode representing the change in OH^- concentration near the electrode during the formation of the NiOOH species [26]. Another negative-going peak is seen at 1470 cm^{-1}, which represents cleavage of the C–N bonds (see Table 2). For the Ni-WC/C catalyst, both negative bands appear at 0.40 V, which is ~50 mV lower than those on the Ni/C catalyst. This implies that the C–N bond can be more easily broken on Ni-WC/C surfaces, thus leading to a lower overpotential of urea electrooxiation. Simultaneously, three positive-going peaks at 2168 cm^{-1}, 1380 cm^{-1} and 1234 cm^{-1} can be detected, which are related to formation of species during the urea oxidation. Among these, the band located at 1380 cm^{-1} corresponds to CO_3^{2-}, confirming the formation of CO_2, which reacts with OH^- to produce carbonate ions in the solution of high pH. At higher potentials, as more CO_2 is produced, a pronounced HCO_3^- band at 1234 cm^{-1} is also observed.

The assignment of the positive band at 2168 cm^{-1} that appears at high potential is challenging since several bands have been reported near this region (e.g. adsorbed CO on Ni [35] and N-bonded NCO groups in typical complexes [36]). As a common intermediate on many metal surfaces during oxidation of various fuels, CO is thus among the possibilities [26]. The CO band should appear at a higher frequency than on metallic Ni because in the alkaline environment Ni is in a higher oxidation state (Ni^{2+} or Ni^{3+}) [37]. It is expected that the frequency of the CO adsorbed on an electrode surface should shift as the potential becomes more positive, due to changes in surface CO coverage and the electron donation from the electrode surface to the adsorbed CO [38]. However, no shift in frequency in the FTIR spectra with the potential is observed, as shown in Fig. 2. Furthermore, the fact that the peak appears at the same frequency on different catalysts suggests that the species may not be the adsorbed ones. In order to confirm its nature, in situ FTIR study was conducted on Ni/C during the CO stripping measurement. As shown in Fig. 3a, no bands were observed between 2200 and 1900 cm^{-1}, indicating that the 2168 cm^{-1} band is not related to adsorbed CO.

Species adsorbed on a metal surface interact with the component of the IR light that is parallel to the plane of incidence (*p*-polarized light), so the adsorbed species must have a dipole moment component perpendicular to the metal surface [39,40]. This surface selection rule does not apply to randomly-oriented solution species, which interact with both *s*- and *p*-polarized IR radiation. To distinguish whether the species producing the 2168 cm^{-1} band is adsorbed on the electrode or in the solution, in situ FTIR spectra during urea oxidation on Ni/C were collected using *s*-polarized IR radiation. The positive-going band centered at 2168 cm^{-1} can still be observed in Fig. 3b, confirming that this feature belongs to species in the solution rather than an adsorbed reaction intermediate. Previous DFT calculations by Botte et al. proposed that cyanate (NCO-) might be produced in one possible pathway during urea oxidation [28]. However, direct detection on this product has not been reported. To validate this assumption, the ATR-IR spectrum of 0.1 M KCNO + 1 M KOH solution, referenced to 1 M KOH, was obtained. As shown in Fig. 3c, the observation of the band at identical frequency of 2168 cm^{-1} confirmed that this feature is related to NCO^-. The formation of cyanate ion indicates a partial oxidation of urea in which only one C–N bond was cleaved.

For the Ni/C catalyst, the increase of NCO^- became more progressive at potential higher than 0.6 V while the intensities of the CO_3^{2-} and HCO_3^- peaks decreased. It is probably due to the strong adsorption (poisoning) of certain intermediates on that surface with the reaction proceeds, and the remaining active sites would prefer the partial oxidation pathway of urea molecules to produce NCO^-, which hinders the complete oxidation to CO_2. Previous studies hypothesized that CO groups might be poisoning the active sites [15,28] but weak of evidence. However, the absence of CO bands in our in situ FTIR study suggests that surface poisoning should be ascribed to species other than CO. Since no other persistent bands can be observed in the spectra, the poisoning intermediates are likely IR insensitive.

Identification of the strongly bound intermediates is difficult using in situ FTIR due to the surface dipole selection rule that precludes the observation of all IR-sensitive bands. However, since the main apparent solution band in the oxidation of urea is cyanate ion, it is likely that its production should be also observed at the electrode. The linear NCO group is a bidentate ligand and may coordinate to a metal through the nitrogen or oxygen atoms, or both. While majority of the cyanato-metal complexes are N-bonded [36], Ni is known to be among a group of metals that can coordinate through both atoms [41]. The bridging structure of NCO on the Ni surface (Ni—N—C—O—Ni) would have both ν(CN) and ν(CO) stretching modes practically parallel to the metal surface (assuming small difference in bond lengths of Ni—O and Ni—N) and therefore forbidden by the surface selection rule. However, this hypothesis is yet to be confirmed by other spectroscopic techniques.

Contrary to Ni/C, all the positive-going bands on Ni-WC/C catalyst continue to grow as the potential increases, suggesting lower adsorption energies of the intermediates. Furthermore, the CO_3^{2-} and HCO_3^- band intensities increased initially and then kept stable as the potential goes positively, also indicating that the reaction pathway toward CO_2 is maintained. The synergic effect between Ni and WC possibly alleviated the poisoning issue according to the relatively stable CO_3^{2-} + HCO_3^- total band intensity at the high potential region. As a result, the higher energy conversion efficiency can be achieved following the complete oxidation pathway of urea that yields N_2 and CO_2 [26]. This is also consistent with the observation that C–N bond can be more easily broken on Ni-WC/C surfaces.

The combined results from Figs. 1 and 2 suggest that the oxidation kinetics depends on two factors: the predominant pathway during oxidation, and adsorption strength of intermediates at the electrode surface. It is likely that the predominant oxidation pathway on the Ni/C electrode is the partial oxidation that leads to the production of NCO^- ion. The partial oxidation yields lower current densities, in agreement with the sluggish urea oxidation on Ni/C. On the other hand, the observation of approximately 4.5 times higher current density on the Ni-WC/C catalyst, together with the behavior of carbonate/bicarbonate FTIR bands, indicates that the complete oxidation becomes the predominant pathway for urea oxidation on the WC-modified Ni surface. The much higher activity and stability of Ni-WC/C toward urea oxidation can be ascribed to both the easier C–N bond cleavage and anti-poisoning ability caused by the interaction between Ni and WC.

4. Conclusions

The Ni-WC/C catalyst prepared by a sequential impregnation led to enhanced activity and stability for urea electrooxidation, compared to Ni/C at the same Ni loading for urea electrooxidation. With respect to the Ni/C catalyst, the mass activity, electrochemical active surface area and specific activity all increased on the Ni-WC/C electrode. The formation of CO_3^{2-} and NCO^- were detected and the synergistic effect of Ni and WC was investigated. The in situ FTIR results revealed that the C–N bond scission occurred more easily on Ni-WC/C than on Ni/C, resulting in a lower overpotential. Furthermore, the higher activity and stability on Ni-WC/C catalyst would also be attributed to the enhanced anti-poisoning of Ni-based catalysts leading to the more complete

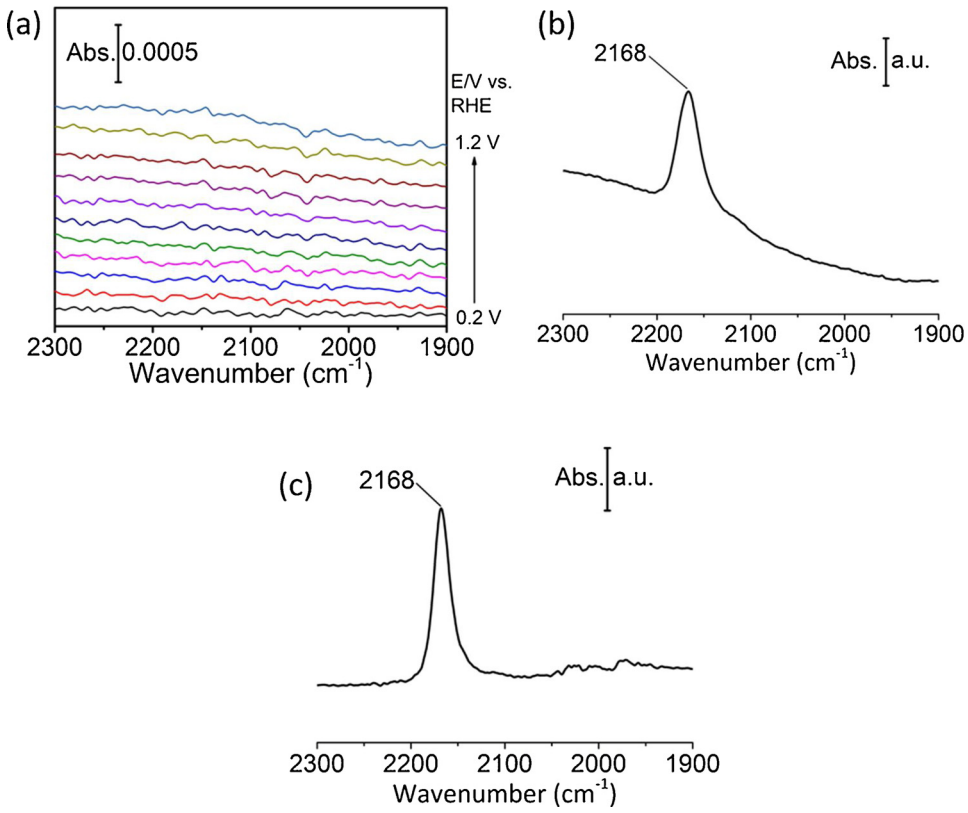

Fig. 3. (a) Real-time IR spectra collected during the CO stripping measurement on Ni/C. IR reference was taken at 0.1 V vs RHE. (b) IR spectrum collected at 0.7 V vs Hg/HgO during the urea oxidation reaction on Ni/C under s-polarized IR beam. (c) The ATR-IR spectrum of 0.1 M KCNO + 1 M KOH solution, referenced to 1 M KOH solution.

oxidation of urea to produce CO_2. The current study of the Ni and WC synergistic effect should help design effective catalysts for urea electrooxidation, as well as for the design of Ni-based catalysts for other electrochemical systems.

Acknowledgments

This work was supported by the US Department of Energy, Basic Energy Science, Catalysis Program (DE-FG02-13ER16381). The work at the Hong Kong University of Science and Technology was supported by Research Grant Council (26206115 and 16304117) of the Hong Kong Special Administrative Region.

References

[1] Z.W. Seh, et al., Combining theory and experiment in electrocatalysis: insights into materials design, Science 355 (6321) (2017) p. eaad4998.
[2] R. Bashyam, P. Zelenay, A class of non-precious metal composite catalysts for fuel cells, Nature 443 (7107) (2006) 63–66.
[3] A.N. Rollinson, et al., Urea as a hydrogen carrier: a perspective on its potential for safe, sustainable and long-term energy supply, Energy Environ. Sci. 4 (4) (2011) 1216–1224.
[4] B.K. Boggs, R.L. King, G.G. Botte, Urea electrolysis: direct hydrogen production from urine, Chem. Commun. 32 (2009) 4859–4861.
[5] R. Lan, S.W. Tao, J. Irvine, A direct urea fuel cell – power from fertiliser and waste, Energy Environ. Sci. 3 (4) (2010) 438–441.
[6] W. Xu, et al., Nickel-cobalt bimetallic anode catalysts for direct urea fuel cell, Sci. Rep. 4 (1) (2014) 5863–5868.
[7] S.J. Ewing, et al., Synthesis of dendritic nano-sized nickel for use as anode material in an alkaline membrane fuel cell, Fuel Cells 10 (1) (2010) 72–76.
[8] W. Xu, Z. Wu, S. Tao, Urea-based fuel cells and electrocatalysts for urea oxidation, Energy Technol. 4 (11) (2016) 1329–1337.
[9] R. Lan, S. Tao, Preparation of nano-sized nickel as anode catalyst for direct urea and urine fuel cells, J. Power Sources 196 (11) (2011) 5021–5026.
[10] V. Vedharathinam, G.G. Botte, Understanding the electro-catalytic oxidation mechanism of urea on nickel electrodes in alkaline medium, Electrochim. Acta 81 (2012) 292–300.
[11] D. Wang, et al., Electrochemically reduced graphene oxide–nickel nanocomposites for urea electrolysis, Electrochim. Acta 89 (2013) 732–736.
[12] D. Wang, W. Yan, G.G. Botte, Exfoliated nickel hydroxide nanosheets for urea electrolysis, Electrochem. Commun. 13 (10) (2011) 1135–1138.
[13] W. Yan, et al., Nickel nanowires as effective catalysts for urea electro-oxidation, Electrochim. Acta 134 (2014) 266–271.
[14] R. Ji, et al., Formation of open-ended nickel hydroxide nanotubes on three-dimensional nickel framework for enhanced urea electrolysis, Electrochem. Commun. 29 (2013) 21–24.
[15] R.L. King, G.G. Botte, Investigation of multi-metal catalysts for stable hydrogen production via urea electrolysis, J. Power Sources 196 (22) (2011) 9579–9584.
[16] A.T. Miller, B.L. Hassler, G.G. Botte, Rhodium electrodeposition on nickel electrodes used for urea electrolysis, J. Appl. Electrochem. 42 (2012) 925–934.
[17] W. Yan, D. Wang, G.G. Botte, Nickel and cobalt bimetallic hydroxide catalysts for urea electro-oxidation, Electrochim. Acta 61 (2012) 25–30.
[18] C.J.F.C. Mao-Sung Wu, Carbon-encapsulated nickel-iron nanoparticles supported on nickel foam as a catalyst electrode for urea electrolysis, Electrochim. Acta 227 (2017) 210–216.
[19] N.A.M. Barakat, et al., Enhanced onset potential NiMn-decorated activated carbon as effective and applicable anode in urea fuel cells, Catal. Commun. 97 (2017) 32–36.
[20] W. Shi, et al., Enhanced performance and electrocatalytic kinetics of Ni-Mo/graphene nanocatalysts towards alkaline urea oxidation reaction, Electrochim. Acta 242 (2017) 247–259.
[21] W. Yan, D. Wang, G.G. Botte, Electrochemical decomposition of urea with Ni-based catalysts, Appl. Catal. B: Environ. 127 (2012) 221–226.
[22] S.T. Hunt, et al., Self-assembly of noble metal monolayers on transition metal carbide nanoparticle catalysts, Science 352 (6288SI) (2016) 974–978.
[23] Y. Xiao, J. Hwang, Y. Sun, Transition metal carbide-based materials: synthesis and applications in electrochemical energy storage, J. Mater. Chem. A 4 (27) (2016) 10379–10393.
[24] S.T. Hunt, T. Nimmanwudipong, Y. Román-Leshkov, Engineering non-sintered, metal-terminated tungsten carbide nanoparticles for catalysis, Angew. Chem. Int. Ed. (2014) 5131–5136.
[25] L. Wang, et al., Ni-WC/C nanocluster catalysts for urea electrooxidation, J. Power Sources 264 (2014) 282–289.
[26] V. Vedharathinam, G.G. Botte, Direct evidence of the mechanism for the electro-oxidation of urea on $Ni(OH)_2$ catalyst in alkaline medium, Electrochim. Acta 108 (2013) 660–665.
[27] D. Wang, G.G. Botte, In situ X-ray diffraction study of urea electrolysis on nickel catalysts, ECS Electrochem. Lett. 3 (9) (2014) H29–H32.
[28] D.A. Daramola, D. Singh, G.G. Botte, Dissociation rates of urea in the presence of NiOOH catalyst: a DFT analysis, J. Phys. Chem. A 114 (43) (2010) 11513–11521.
[29] S. Wasmus, A. Küver, Methanol oxidation and direct methanol fuel cells: a selective review, J. Electroanal. Chem. 461 (1–2) (1999) 14–31.
[30] E.G. Mahoney, et al., Analyzing the electrooxidation of ethylene glycol and glucose over platinum-modified gold electrocatalysts in alkaline electrolyte using in-situ infrared spectroscopy, J. Power Sources 305 (2016) 89–96.
[31] S. Wu, D. Chen, Synthesis and characterization of nickel nanoparticles by hydrazine reduction in ethylene glycol, J. Colloid Interface Sci. 259 (2) (2003) 282–286.

[32] M. Nie, et al., Highly efficient AuPd-WC/C electrocatalyst for ethanol oxidation, Electrochem. Commun. 9 (9) (2007) 2375–2379.
[33] R.L. King, G.G. Botte, Hydrogen production via urea electrolysis using a gel electrolyte, J. Power Sources 196 (5) (2011) 2773–2778.
[34] D. Wang, et al., Enhanced electrocatalytic oxidation of urea based on nickel hydroxide nanoribbons, J. Power Sources 217 (2012) 498–502.
[35] K. Hadjiivanov, H. Knözinger, M. Mihaylov, FTIR study of CO adsorption on Ni-ZSM-5, J. Phys. Chem. B 106 (10) (2002) 2618–2624.
[36] K. Nakamoto, Infrared and Raman Spectra of Inorganic and Coordination Compounds, John Wiley & Sons, Ltd., 2006.
[37] M. Mihaylov, K. Hadjiivanov, FTIR study of CO and NO adsorption and coadsorption on Ni-ZSM-5 and Ni/SiO_2, Langmuir 18 (11) (2002) 4376–4383.
[38] G. Blyholder, Molecular orbital view of chemisorbed carbon monoxide, J. Phys. Chem. 68 (10) (1964) 2772–2777.
[39] D. Cozzolino, Infrared Spectroscopy: Theory, Developments and Applications, (2013), pp. 307–332.
[40] R.G. Greenler, Infrared study of adsorbed molecules on metal surfaces by reflection techniques, J. Chem. Phys. 44 (1966) 310–315.
[41] Z. Mahendrasinh, et al., Cyanato bridged binuclear nickel(II) and copper(II) complexes with pyridylpyrazole ligand: synthesis, structure and magnetic properties, Inorg. Chim. Acta 375 (1) (2011) 333–337.
[42] V. Climent, et al., On the electrochemical and in-situ Fourier transform infrared spectroscopy characterization of urea adlayers at Pt(100) electrodes, Langmuir 13 (8) (1997) 2380–2389.
[43] V. Climent, et al., Urea adsorption on Pt(111) electrodes, J. Electroanal. Chem. 461 (1–2) (1999) 65–75.
[44] P. Fischer, C.A. Mcdowell, The infrared absorption spectra of urea-hydrocarbon adducts, Can. J. Chem. 38 (2) (1960) 187–193.
[45] E.E. Coleyshaw, G. Crump, W.P. Griffith, Vibrational spectra of the hydrated carbonate minerals ikaite, monohydrocalcite, lansfordite and nesquehonite, Spectrochim. Acta Part A: Mol. Biomol. Spectrosc. 59 (10) (2003) 2231–2239.
[46] E. Garand, et al., Infrared spectroscopy of hydrated bicarbonate anion clusters: $HCO_3^-(H_2O)_{1-10}$, J. Am. Chem. Soc. 132 (2) (2010) 849–856.